The influence of substrate orientation on the magnetic behavior of nearly-stoichiometric Mn5Ge3 thin films: DFT calculations and experimental analysis

R.C. Oliveira, Massimiliano Marangolo, D.H. Mosca, J. Varalda

The influence of substrate orientation on the magnetic behavior of nearly-stoichiometric Mn_5Ge_3 thin films: DFT calculations and Experimental analysis

R. C. Oliveira[1], M. Marangolo[2], D. H. Mosca[1], J. Varalda[1]

[1] Departamento de Física, Universidade Federal do Paraná, Caixa Postal 19044, CEP 81531-990, Curitiba, Paraná, Brasil.
[2] Sorbonne Université, CNRS, Institut des NanoSciences de Paris, UMR7588, F-75252, Paris, France

Abstract

The Mn_5Ge_3 exhibits a wide range of fascinating properties such as high spin polarization up to 42%, large spin diffusion lengths, near-room Curie temperature, and possible integration with Ge, GaAs, and Si substrates. The influence of substrate orientation on magnetic behavior has been investigated. The thin films studied present an in-plane magnetic reversal which is isotropic in samples grown on GaAs(111) and anisotropic in samples grown on GaAs(001). Another difference observed is a linear trend to saturation on the out-of-plane hysteresis loop in samples grown on GaAs(111), comparatively to samples grown on GaAs(001). To better understand this scenario, Density Functional Theory (DFT) calculations were conducted. The results indicate a ferromagnetic metallic ground state with properties that are consistent with the experimental results. The projected densities of states indicate that the main responsible for the magnetic moment observed in the Mn_5Ge_3 is the Mn-Mn interaction. The magnetic field distribution isosurfaces obtained from the DFT calculations offer a satisfactory explanation of the magnetic reversal experimentally observed, especially the in-plane magnetic behavior in samples grown on both GaAs(111) and GaAs(001) substrates. This work provides a theoretical-experimental approach that allows a deeper understanding of the magnetic anisotropy behavior under the influence of the crystallographic orientation of the substrate observed in nearly-stoichiometric Mn_5Ge_3 thin films, which is a good candidate for rare-earth free magnet in spintronic applications.

Introduction

The intermetallic compound Mn_5Ge_3 has good potential for spintronic applications due to some attractive structural, electronic, and magnetic properties. These properties include but are not limited to, high spin polarization up to 42% [1], large spin diffusion lengths [2], near-room Curie temperature (Tc) [3] and the possibility of integration with Ge [4,5], GaAs [6], and Si [7] substrates. Such physical properties are favorable to a number of applications and have drawn a lot of attention to this alloy.

Spintronic devices utilize the spin of the electron as a degree of freedom [8]. Nowadays, the merging of spintronics and magnetothermodynamics in the field called spincaloritronics has growing importance. We have demonstrated that the Mn5Ge3 films are possible candidates for magnetic refrigeration while being a rare earth-free material, gathering a multifunctional potential in spintronics and spincaloritronics [6]. In these scenarios, magnetic anisotropy plays an important role in determining the magnetic functionality of spintronic devices [8].

Bulk Mn_5Ge_3 has a hexagonal crystal structure of the $D8_8$ type (space group $P6_3/mcm$) with unit cell lattice parameters $a = 7.184\ \text{Å}$ and $c = 5.053\ \text{Å}$. It is ferromagnetic with a Curie temperature of $Tc = 304\ K$ and an easy magnetization axis along the *c* axis [9]. There are two crystallographically distinct sets of manganese in this cell, named Mn-type I and Mn-type II. The Mn-type I atoms are in four-fold positions with 32 symmetry and the Mn-type II are in six-fold positions with mm symmetry.

In a recent work [6] we studied some magnetic properties of nearly-stoichiometric Mn_5Ge_3 thin films on GaAs(001) and GaAs(111). While the bulk Mn_5Ge_3 has an easy magnetization axis along the c axis, we have shown that in the form of thin film this is not observable.

The present work aims to further investigate the magnetic properties of this alloy providing a deeper

understanding of magnetic anisotropies and magnetic reversal behavior observed in these thin films.

Methods

Mn_5Ge_3 thin films were grown by the co-deposition of Mn and Ge in a molecular beam epitaxy (MBE) chamber. The deposition was done on commercial epi-ready GaAs wafers for one hour with subsequent annealing for one hour. In both procedures, the substrate was kept at 200 °C. The Ge effusion cell temperature was kept fixed at 1100 °C for all samples, meanwhile, the temperature of the Mn effusion cell was changed from one sample to another, and their values are shown in Table 1. The resulting single-phase films are highly textured crystals with a preferential alignment and a thickness ranging from 71 up to 88 nm. The following epitaxial relationships for the thin films grown on GaAs (111) were obtained from X-ray diffraction (XRD) analysis (not shown):

- (001) Mn_5Ge_3 // (111) GaAs
- [110] Mn_5Ge_3 // [2-1-1] GaAs

And for the samples grown on GaAs(001):

- (111) Mn_5Ge_3 // (001) GaAs
- [-110] Mn_5Ge_3 // [110] GaAs

Further growth condition details and structural characterizations are explained elsewhere [6].

Table 1 – Nomenclature of samples and their composition obtained from the growth procedures using different Mn effusion cell temperatures. All the samples were grown with the Ge effusion cell at 1100 °C. The samples named Sn_{111} (n = 1 or 2) were grown on GaAs(111), while the ones named Sn_{001} (n = 1 or 2) were grown on GaAs(001).

Sample	Mn temperature (°C)	Stoichiometry
$S1_{111}$	800	$Mn_{4.6}Ge_{3.4}$
$S2_{111}$	820	$Mn_{4.9}Ge_{3.1}$
$S1_{001}$	800	$Mn_{5.1}Ge_{2.9}$
$S2_{001}$	820	$Mn_{5.5}Ge_{2.5}$

The magnetic properties were determined using a physical property measurement system (PPMS Quantum Design) equipped with the vibrating sample magnetometer (VSM) option. All the hysteresis loops were measured at 10 K. These magnetic measurements were done along three distinct crystallographic directions of GaAs substrates, two along the film plane and another perpendicular to the film plane. To better understand the magnetic behavior of the samples, DFT calculations were made using all-electron Full Potential Linearized Augmented Plane Wave (FP-LAPW) method as implemented in ELK code [10]. These calculations were done using the experimental lattice parameters found through x-ray diffraction measurements using a supercell with a total of 16 atoms, shown in Figure 4, to better represent the Mn_5Ge_3 stoichiometry. We used GGA exchange-correlation functional within the PBEsol approximation [11] for the non-collinear spin-polarized calculations (spin-orbit coupling included). The total energy and the Kohn-Sham potential and field convergences were better than $1x10^{-5}$ Ha and $1x10^{-7}$ Ha, respectively. The exchange-correlation magnetic vector field isosurfaces were first visualized using VESTA [12] and later exported to Blender [13] to combine and color the isosurfaces from different atoms. This exchange-correlation field [14,15] has its direction along the direction of the local spin density and helps the observation of the magnetic axis. Hereafter, the exchange-correlation vector field isosurfaces is referred as magnetic field distribution (MFD) isosurfaces.

Results and discussions

For an easier understanding, the following notations will be used: $[uvw]_S$ when referring to the substrate crystallographic directions; and $[uvw]_F$ when referring to the film crystallographic directions. The results of the magnetic measurements shown have already had the diamagnetic contribution from the substrate subtracted.

The samples $S1_{111}$ and $S2_{111}$ have very similar magnetic behavior, as shown in Figure 1. In both samples, magnetic isotropy can be observed in the in-plane crystallographic directions ($[01\text{-}1]_S$ and $[2\text{-}1\text{-}1]_S$).

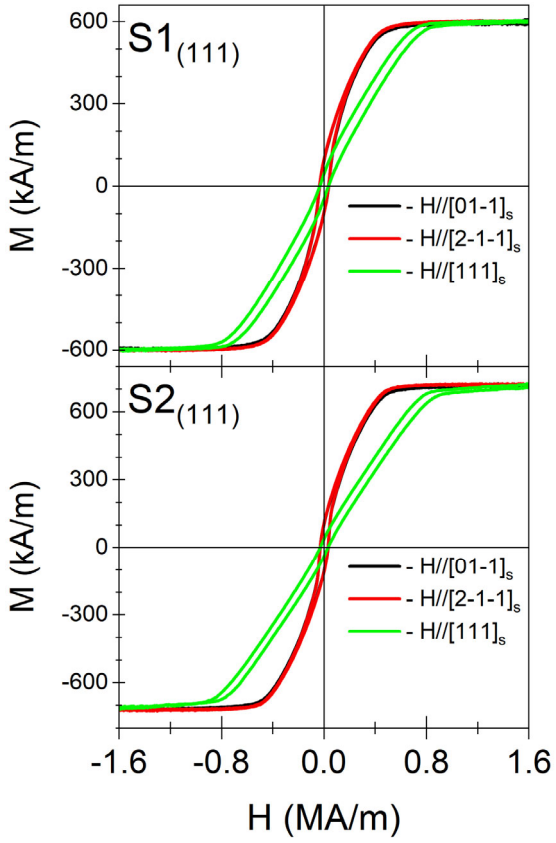

Figure 1 – Hysteresis loops of Mn_5Ge_3/GaAs(111) thin films measured at 10 K with magnetic field applied along the substrate directions as indicated.

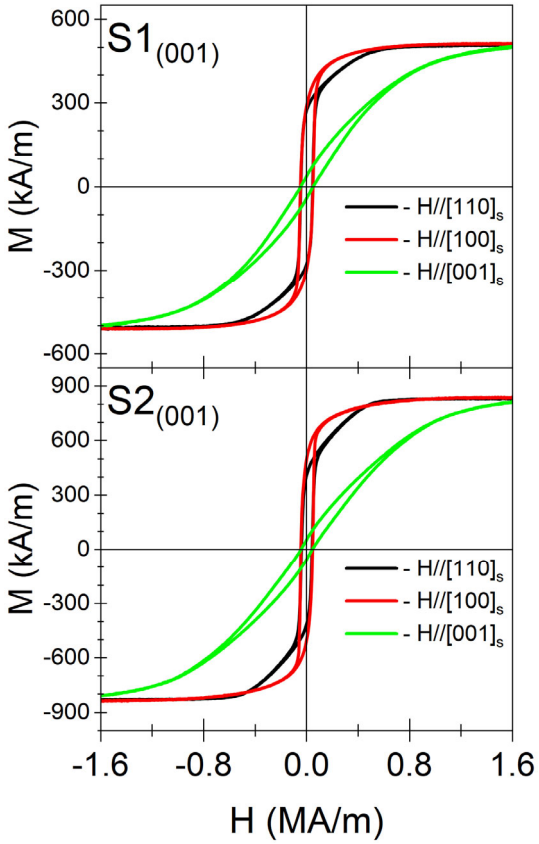

Figure 2 – Hysteresis loops of Mn_5Ge_3/GaAs(001) thin films measured at 10 K with magnetic field applied along the substrate directions as indicated.

In the out-of-plane direction ($[111]_S$), it can be observed a magnetic behavior in which the magnetization increases linearly with the applied magnetic field going to saturation magnetization values. This linear magnetic behavior is also observed in the in-plane directions, but the magnetic field range in which this linear behavior can be observed is smaller when compared with the out-of-plane direction. This implies an in-plane magnetization reversal and small remanence relative to saturation magnetization which is often associated with a striped magnetic domain structure [16,17], whose magnetization components point in-plane and out-of-plane. However, only a weak stripe domain structure is reported in Mn_5Ge_3 epitaxial films grown on Ge(111) substrates [18,19].

The linear magnetic response observed in the Mn_5Ge_3/GaAs(111) samples is not present in the samples grown on GaAs(001) substrates. Another distinctive feature is the in-plane magnetic anisotropy with an easier axis along the $[100]_S$ crystallographic direction, observed in both samples $S1_{001}$ and $S2_{001}$. The samples grown on GaAs(001) also have a higher in-plane remanent magnetization as well as higher coercive fields when compared with those grown on GaAs(111).

Independently of the substrate orientations, the magnetic moment increases as a function of the Mn content in the films, indicating their crucial role in the alloying. Similar behavior has been observed in off-stoichiometric $Mn_{5+x}Ge_{3-x}$ ingots [20]. The overall mean value of 2.6 μ_B/Mn atom as well as the magnetic moment values obtained for Mn-type I and Mn-type II sites in the DFT calculations are in good agreement with results found in the literature [21]. The DFT results also show that there is a negative but small magnetic moment related to the Ge sites. The experimental variations in both lattice parameters and stoichiometry lead to similar results in the calculations with no significant differences (not shown).

Table 2 – Magnetic moment obtained from the experimental results and DFT calculations.

Sample	**Magnetic moment (μ_B/Mn atom)**
$S1_{111}$	1.55
$S2_{111}$	1.74
$S1_{001}$	1.19
$S2_{001}$	1.81
DFT	**Magnetic moment (μ_B)**
Mn-type I	2.18
Mn-type II	3.07

Ge	-0.12
Overall cell	2.6

The analysis of the total density of states (DOS) in Figure 3-a) reveals a metallic ground state with magnetic properties that are consistent with electrical resistivity and magnetic experiments found in the literature [3,22], as well as with the magnetic results reported in this paper. The projected density of states (PDOS) due to Mn sites, Figure 3-b), is dominated by Mn *d* states since the contributions from *s* and *p* states (not shown) are negligible. A quite large Mn-Mn interaction can be observed close to the Fermi level while a small hybridization between Ge *p* and Mn *d* states can be observed at higher-binding energy ranges. As expected, a difference in the PDOS of Mn-type I and Mn-type II is observed, especially in the majority spin-subband, as it has already been observed [21]. The minority spin-subband shows minor differences between Mn-type I and Mn-type II, and it is the dominant contribution to the unoccupied states. The main contribution from the Ge atom is the 4p state. It can be observed that the Ge-4p is delocalized with a small PDOS value and the majority and minority spin-subbands are inverted when compared with Mn-type I and Mn-type II *d* states. The hybridization between Mn *d* and Ge *p* states gives origin to the small Ge magnetic moment of -0.12 μB, indicating that the fundamental magnetic order of the Mn_5Ge_3 is ferrimagnetic. However, with such a small magnetic moment associated with the Ge atom, a ferromagnetic order can be considered a good approximation.

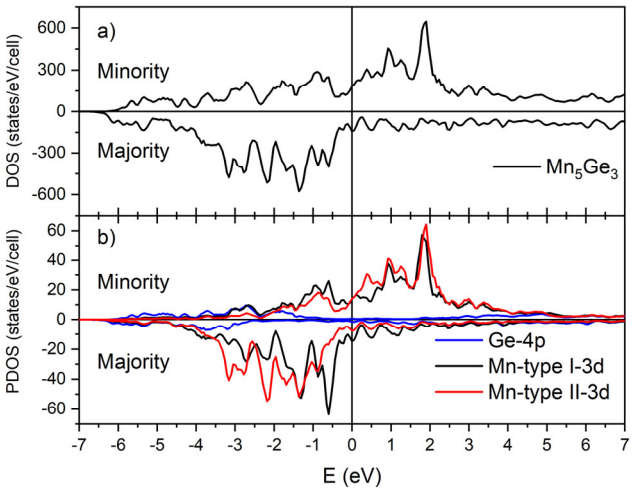

Figure 3 – a) Mn_5Ge_3 total density of states (DOS) and b) the projected density of states (PDOS) of Ge, Mn-type I, and Mn-type II. The minority (majority) spin-subband is shown in the positive (negative) y-axis. The zero on the energy scale represents the Fermi energy (E_F).

Another important result obtained from the DFT calculations are the magnetic field distribution isosurfaces. Figure 4 shows illustrations of the Mn_5Ge_3 16 atoms structure used for the calculations and its representative MFD isosurfaces.

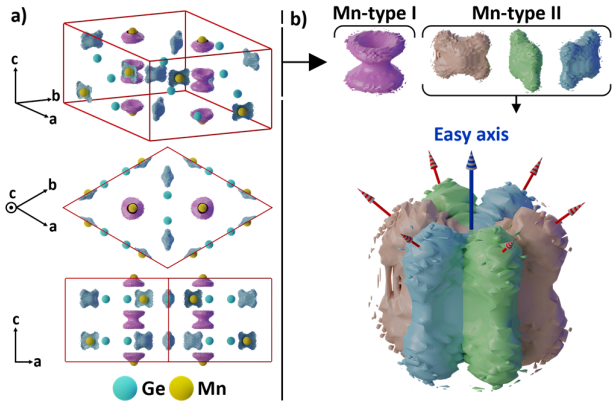

Figure 4 – a): Illustration of the Mn_5Ge_3 16 atoms structure used for the calculations and its representative MFD isosurfaces. The light blue and yellow spheres represent the Ge and Mn atoms, respectively. This image shows two different isosurfaces, 0.0065 and 0.0092 a.u. to facilitate the visualization of the characteristic Mn-type I (pink) and Mn-type II (blue) isosurfaces, respectively. Notably, the Mn-type II MFD isosurfaces exhibit different alignments relative to the unit cell. B): the Mn-type I and all the possible alignments of the Mn-type II isosurfaces individually shown for batter visualization. The Mn-type II have lobes forming a 50° angle with the out-of-plane c direction, their direction is indicated with red arrows. A superposition of these three possible alignments reveals a resultant vector along the c direction, indicating the direction of the easy magnetization axis. Design resources of Blender [13] *software was used in the illustration production.*

The MFD isosurfaces shown in the panel a) of Figure 4 have two distinct characteristic shapes visualized respectively by pink and blue colors, representing the magnetic field distribution of the Mn-type I and Mn-type II sites. These MFD isosurfaces are individually shown in the panel b) of Figure 4 to better show their distinct shapes. The Mn-type I MFD has two conic nodules mirrored along the *c* direction and, therefore, it is isotropic along the *a*-*b* plane. According to this observation, the magnetization process for magnetic fields applied along these orientations are expected to be quite similar. Due to the conic symmetry, the easy magnetic axis for these atoms has its direction along the *c* direction. Meanwhile, the MFD isosurfaces around Mn-type II sites has a spheroidal shape distorted by lobes forming an X-like shape. These lobes are inclined at a 50° angle in relation to the *c* crystallographic direction. Notably, the Mn-type II isosurfaces exhibit three distinct alignments relative to the unit cell. When examining each of these alignment in isolation, it becomes evident that the local easy axis is oriented towards the lobes at the previously mentioned 50° angle from the *c* direction. However, a more comprehensive perspective emerges when considering the amalgamation of all possible alignments (as depicted on the panel b) of Figure 4). This comprehensive view

highlights a resultant vector, represented by the blue arrow, arising from the summation of these individual local easy axes denoted by red arrows. This composite vector indicates a direction pointing towards the *c* orientation. As a direct consequence, the inherent easy magnetic axis of the unit cell, align in the direction of the *c* axis.

To draw meaningful comparisons between these isosurfaces and the experimental results, its necessary to account for the epitaxial relationship between the film and the underlying substrate. The illustration presented in Figure 5 provides a superposition of the three alignments inherent to the Mn-type II MFD isosurfaces. This depiction also encompasses the orientations of both the thin film and the substrate for both GaAs(001) and GaAs(111) crystallographic planes. Given the simpler geometry of the Mn-type I shape, and the fact that the cone generatrix within it shares the identical 50° inclination observed in the lobes of the Mn-type II, all the conclusions drawn from the analysis of the Mn-type II MFD isosurfaces hold true for their Mn-type I counterparts as well.

The similarity between the $[110]_F//[2\text{-}1\text{-}1]_S$ and the $[\text{-}110]_F//[01\text{-}1]_S$ directions in the Mn-type II sites for samples grown on GaAs(111), shown in Figure 5, combined with the in-plane isotropic shape of Mn-type I sites shown in Figure 4, corroborate the experimental in-plane isotropic data presented in Figure 1. The DFT results for the samples grown on GaAs(001) also satisfactorily explain the experimental magnetic behavior observed. The MFD isosurfaces for Mn-type II sites shown in Figure 5 indicate that there are stable magnetic axes along the $[01\text{-}1]_F//[100]_S$ and $[111]_F//[001]_S$ directions, while the $[\text{-}110]_F//[110]_S$ direction is along a medium axis, between an easy and a hard magnetization axis. Therefore, it is expected that the $[01\text{-}1]_F//[100]_S$ direction is easier to magnetize when compared with the $[\text{-}110]_F//[110]_S$ crystallographic direction. Again, this observation is in good agreement with the experimental results shown in Figure 2.

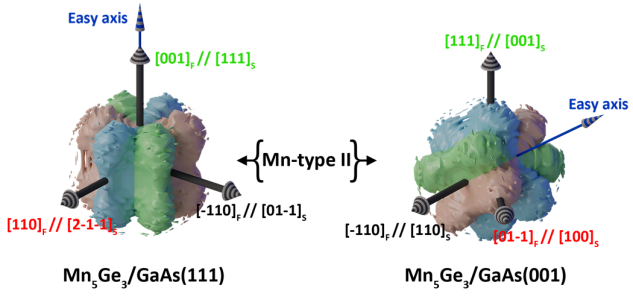

Figure 5 –Superposition of MFD isosurfaces for Mn_5Ge_3 with the crystal orientations of the GaAs substrates. The MFD isosurface around Mn-type II sites shown is the superposition of all possible symmetry trends of the isosurfaces that this magnetic field distribution has in the Mn_5Ge_3 alloy. The representative isosurfaces are colored with distinct colors for easier visualization. The isosurfaces have been obtained by DFT calculations and posteriorly exported to Blender [13] to combine the different spatial alignment of the MFD isosurfaces of Mn-type II site in the supercell.

The crystallographic directions $[01\text{-}1]_S$ for GaAs(111) and $[110]_S$ for GaAs(001) correspond to the same $[\text{-}110]_F$ direction, as can be observed in Figure 5. Comparing these two directions in Figure 1 and Figure 2, similar magnetic processes can be observed. Essentially, starting from the remanent magnetization, the magnetization tends to increase almost linearly towards saturation when applying the magnetic field along these crystallographic directions in both substrates.

Figure 5 also reveals that the perpendicular direction $[111]_F//[001]_S$ for the Mn_5Ge_3 grown on GaAs(111) is along the easy magnetization axis, which is not true for the samples grown on GaAs(001). As such, it is expected that along the perpendicular direction is easier to magnetize samples grown on GaAs(111) than those grown on GaAs(001). This can be observed in Figure 1 and Figure 2. In the out-of-plane direction, the samples grown on GaAs(111) have a lower saturation magnetic field (HS) than that observed in GaAs(001). As such, the DFT calculations agree with the experimental data.

Although the *c* axis is qualified as the easy axis of magnetization in this system, the measurement with a magnetic field applied in this direction shows a hard axis compared to those associated with the film plane (Figure 1). A possible explanation for this is the contribution of the shape (magnetostatic) anisotropy (K_s) component that is not computed in the DFT calculations. In a thin film with the magnetic field applied in the normal direction of the film plane, the K_s values can be estimated using: $K_s = -\frac{\mu_0}{2} M_s^2$, where M_S is the saturation magnetization. Meanwhile, the uniaxial anisotropy (K_u) was estimated calculating the difference between the areas under the magnetization curves with the magnetic field applied in the $[2\text{-}1\text{-}1]_S$ and $[111]_S$, for the samples grown on GaAs(111) and $[100]_S$ and $[001]_S$, for the samples grown on GaAs(001). The results of these estimates are shown in Table 3. The absolute values of the shape anisotropy K_s and the uniaxial anisotropy K_u indicates that the shape anisotropy is either dominant or comparable with K_u in the samples. This observation might explain the out-of-plane hard magnetization axis obtained in the experimental measurements. From DFT, K_u can be calculated as the energy difference between [001] (easy) and the other important axes as [100], [110] and [011]. The values are very close along the different

orientations, varying only between 0.21 and 0.25 MJ/m^3. The experimentally observed values of K_u are in good agreement with those obtained from the DFT calculations, especially the samples closest to the Mn_5Ge_3 stoichiometry. The samples that present the biggest deviation from this theoretical K_u value, namely $S1_{111}$ and $S2_{001}$, also have the biggest deviation from the Mn_5Ge_3 stoichiometry, meaning that this difference probably arises from the higher chemical disorder present in these samples.

Table 3 – Shape anisotropy constant K_s, uniaxial anisotropy constant K_u. For the calculation of K_u by DFT, no additional convergence tests were carried out. The same ones declared in the methods section were used. Although the data obtained are consistent with the qualitative analysis based on MFDs isosurfaces as well as with the values obtained experimentally, their absolute values may vary in a more rigorous calculation.

Sample	K_s (x10^5 J/m^3)	K_u (x10^5 J/m^3)	$K_u(DFT)$ (x10^5 J/m^3)
$S1_{111}$	-2.3	1.2	2.1 – 2.5
$S2_{111}$	-3.3	2.1	
$S1_{001}$	-1.7	2.6	2.1 - 2.5
$S2_{001}$	-4.4	4.7	

Conclusion

The PDOS analysis indicates that the magnetic moment observed in the Mn_5Ge_3 based alloy films is mainly due to the Mn-Mn interaction. An increase in the Mn-Mn ferromagnetic interactions as Mn atoms occupies the type-II sites might explain the observation that the magnetic moment increases with an increase in Mn content in the alloy. While Mn atoms increased by 0.3 and 0.4 in the S_{111} and S_{001} sample sets respectively, the corresponding magnetic moments have increased by 0.19 μ_B/Mn atom and 0.62 μ_B/Mn atom. The growth texture induced by substrate orientation appears to favor the filling of type-II sites with increasing Mn concentration. The experimental magnetization curves shown in this paper, together with the DFT results, indicate that our samples present in- and out-of-plane magnetization components. The DFT calculations offer a satisfactory explanation of our experimental results, especially for the in-plane magnetization reversals and small remanence relative to saturation magnetization, mainly in the case of films grown on the GaAs(111) substrates. The interrelationship between the symmetry of the magnetic field distributions calculated by *ab initio* and the macroscopic magnetic properties are important to increase the understanding and the ability to optimize the integration with GaAs technology of Mn_5Ge_3 alloys, with versatile potentialities for use in the design of spintronic devices.

Acknowledgments

The authors acknowledge financial support from CAPES and CNPq and the staff of the MPBT (physical properties – low temperature) platform of Sorbonne Université for their technical support. Authors D.H.M. and J.V. acknowledge support of the INCT of Spintronics and Advanced Magnetic Nanostructures (INCT-SpinNanoMag), CNPq 406836/2022-1, and partial financial support from CNPq (404023/2021-5).

[1] R.P. Panguluri, C. Zeng, H.H. Weitering, J.M. Sullivan, S.C. Erwin, B. Nadgorny, Spin polarization and electronic structure of ferromagnetic Mn_5Ge_3 epilayers, Physica Status Solidi (b) 242 (2005) 67–69. https://doi.org/10.1002/pssb.200510030.

[2] J. Tang, C.-Y. Wang, L. Chang, Y. Fan, T. Nie, M. Chan, W. Jiang, Y.-T. Chen, H. Yang, H. Tuan, L. Chen, K.L. Wang, Electrical Spin Injection and Detection in Mn_5Ge_3/Ge/Mn_5Ge_3 Nanowire Transistors, Nano Lett 13 (2013) 4036–4043. https://doi.org/10.1021/nl401238p.

[3] Forsyth, J.B., P.J. Brown, The spatial distribution of magnetisation density in Mn_5Ge_3, Journal of Physics: Condensed Matter 2 (1990) 2713. http://stacks.iop.org/0953-8984/2/i=11/a=014.

[4] J.H. Grytzelius, H.M. Zhang, L.S.O. Johansson, Surface atomic and electronic structure of Mn_5Ge_3 on Ge(111), Phys Rev B 84 (2011) 195306. https://doi.org/10.1103/PhysRevB.84.195306.

[5] L.-A. Michez, A. Spiesser, M. Petit, S. Bertaina, J.-F. Jacquot, D. Dufeu, C. Coudreau, M. Jamet, V. Le Thanh, Magnetic reversal in Mn_5Ge_3 thin films: an extensive study, Journal of Physics: Condensed Matter 27 (2015) 266001. https://doi.org/10.1088/0953-8984/27/26/266001.

[6] R. Cardoso de Oliveira, D. Demaille, N. Casaretto, Y.J. Zheng, M. Marangolo, D.H. Mosca, J. Varalda, Magnetic and structural properties of $Mn_{5+x}Ge_{3+y}$ thin films as a function of substrate orientation, J Magn Magn Mater 539 (2021) 168325. https://doi.org/10.1016/j.jmmm.2021.168325.

[7] I. Yakovlev, I. Tarasov, A. Lukyanenko, M. Rautskii, L. Solovyov, A. Sukhachev, M. Volochaev, D. Efimov, A. Goikhman, I. Bondarev, S. Varnakov, S. Ovchinnikov, N. Volkov, A. Tarasov, Sublayer-Enhanced Growth of Highly Ordered Mn_5Ge_3 Thin Film on Si(111), Nanomaterials 12 (2022) 4365. https://doi.org/10.3390/nano12244365.

[8] A. Hirohata, K. Yamada, Y. Nakatani, I.-L. Prejbeanu, B. Diény, P. Pirro, B. Hillebrands, Review on spintronics: Principles and device applications, J Magn Magn Mater 509 (2020) 166711. https://doi.org/10.1016/j.jmmm.2020.166711.

[9] Y. Tawara, K. Sato, On the Magnetic Anisotropy of Single Crystal of Mn_5Ge_3, J Physical Soc Japan 18 (1963) 773–777. https://doi.org/10.1143/JPSJ.18.773.

[10] K. Dewhurst, S. Sharma, L. Nordström, F. Cricchio, O. Grånäs, H. Gross, Ambrosch-Draxl, C.C. Persson, F. Bultmark, C. Brouder, R. Armiento, A. Chizmeshya, P. Anderson, I. Nekrasov, F. Wagner, Y. Shinohara, The Elk FP-LAPW Code, (n.d.). http://elk.sourceforge.net/.

[11] J.P. Perdew, A. Ruzsinszky, G.I. Csonka, O.A. Vydrov, G.E. Scuseria, L.A. Constantin, X. Zhou, K. Burke, Restoring the Density-Gradient Expansion for Exchange in Solids and Surfaces, Phys Rev Lett 100 (2008) 136406. https://doi.org/10.1103/PhysRevLett.100.136406.

[12] K. Momma, F. Izumi, VESTA 3 for three-dimensional visualization of crystal, volumetric and morphology data, J Appl Crystallogr 44 (2011) 1272–1276. https://doi.org/10.1107/S0021889811038970.

[13] Blender Foundation, Blender - a 3D modelling and rendering package, (2018). http://www.blender.org.

[14] E.A. Pluhar, C.A. Ullrich, Exchange-correlation magnetic fields in spin-density-functional theory, Phys Rev B 100 (2019) 125135. https://doi.org/10.1103/PhysRevB.100.125135.

[15] A. Urru, Lattice dynamics with Fully Relativistic Pseudopotentials for magnetic systems , with selected applications, Doctoral Thesis, Scuola Internazionale Superiore di Studi Avanzati, 2020. https://iris.sissa.it/handle/20.500.11767/115671.

[16] N. Saito, H. Fujiwara, Y. Sugita, A New Type of Magnetic Domain Structure in Negative Magnetostriction Ni-Fe Films, J Physical Soc Japan 19 (1964) 1116–1125. https://doi.org/10.1143/JPSJ.19.1116.

[17] M. Barturen, B. Rache Salles, P. Schio, J. Milano, A. Butera, S. Bustingorry, C. Ramos, A.J.A. de Oliveira, M. Eddrief, E. Lacaze, F. Gendron, V.H. Etgens, M. Marangolo, Crossover to striped magnetic domains in $Fe_{1-x}Ga_x$ magnetostrictive thin films, Appl Phys Lett 101 (2012) 092404. https://doi.org/10.1063/1.4748122.

[18] A. Spiesser, F. Virot, L.-A. Michez, R. Hayn, S. Bertaina, L. Favre, M. Petit, V. Le Thanh, Magnetic anisotropy in epitaxial Mn_5Ge_3 films, Phys Rev B 86 (2012) 035211. https://doi.org/10.1103/PhysRevB.86.035211.

[19] R. Kalvig, E. Jedryka, P. Aleshkevych, M. Wojcik, W. Bednarski, M. Petit, L. Michez, Ferromagnetic resonance in Mn_5Ge_3 epitaxial films with weak stripe domain structure, J Phys D Appl Phys 50 (2017) 125001. https://doi.org/10.1088/1361-6463/aa5ce5.

[20] Y. Kim, E.J. Kim, K. Choi, W.B. Han, H.-S. Kim, C.S. Yoon, Magnetocaloric effect of $Mn_{5+x}Ge_{3-x}$ alloys, J Alloys Compd 620 (2015) 164–167. https://doi.org/10.1016/j.jallcom.2014.09.034.

[21] S. Picozzi, A. Continenza, A.J. Freeman, First-principles characterization of ferromagnetic Mn_5Ge_3 for spintronic applications, Phys Rev B 70 (2004) 235205. https://doi.org/10.1103/PhysRevB.70.235205.

[22] C. Zeng, S.C. Erwin, L.C. Feldman, A.P. Li, R. Jin, Y. Song, J.R. Thompson, H.H. Weitering, Epitaxial ferromagnetic Mn_5Ge_3 on Ge(111), Appl Phys Lett 83 (2003) 5002–5004. https://doi.org/10.1063/1.1633684.